Chemical Physics 325 (2006) 170–177
Preprint of accepted version (online published 6 October 2005)
File generated by M. Hoffmann on 07.06.2006.

Ultrafast relaxation and exciton-exciton annihilation in PTCDA thin films at high excitation densities

E. Engel *, K. Leo, and M. Hoffmann,
Institut für Angewandte Photophysik, Technische Universität Dresden, D-01062 Dresden, Germany

Abstract

Femtosecond pump-probe spectroscopy is applied to thin films of the quasi-one-dimensional organic semiconductor PTCDA (3,4,9,10-perylene tetracarboxylic dianhydride). We present transient absorption spectra over a broad spectral range. Ultrafast intraband relaxation in the S_1 manifold towards the border of the Brillouin zone is shown to depend on temperature and excitation density. The intraband relaxation time is of the order of 100 fs. At high excitation densities ($> 10^{19}\,\mathrm{cm}^{-3}$), the major de-excitation mechanism for the relaxed excitons is exciton-exciton annihilation. The experimental decay dynamics can be very well explained by two alternative annihilation models: one-dimensional diffusion limited bimolecular recombination or single-step long range Förster-type annihilation. In contrast, a three-dimensional diffusion limited annihilation model is significantly inferior. For all three models, we extract annihilation rates, diffusion constants, diffusion lengths, and Förster radii for room and liquid Helium temperature.

Key words: PTCDA, Organic Molecular Crystals, Ultrafast Spectroscopy, Exciton-exciton annihilation, Exciton diffusion
PACS: 71.35.-y, 78.47.+p, 66.30.-h

1. Introduction

Optical properties of organic semiconductors and conjugated polymers have increasingly been subject of many research activities, not only since the first successful presentations of archetypical devices such as organic solar cells [1] or light emitting devices [2]. Still, the numerous degrees of freedom in organic materials hamper the theoretical understanding. One aspect in this complex picture is the interaction between excitons or excitons and charge carriers at high excitation densities, which limits the performance of such devices. Baldo and co-workers have shown how exciton-exciton interaction and annihilation restrains the efficiency of triplet emitter OLED [3] and that singlet-singlet annihilation is a crucial loss mechanism to be overcome in attempts towards electrically pumped organic lasers [4]. Hence, annihilation processes should be understood in detail. In fact, they have been intensively studied during the early works on polyacene single crystals [5], and also in various

---

* Corresponding author. Tel./Fax. +49-351-463-33432/37065
Email address: `engel@iapp.de` (E. Engel).

other materials of current interest, e.g. phthalocyanines [6,7], J-aggregates [8,9], or conducting polymers [10].

However, in the prototypical class of the quasi-one-dimensional perylene derivatives [11], best represented by PTCDA (3,4,9,10-perylene tetracarboxylic dianhydride) [12], there have been only a few recent studies at high excitation densities.

The ultrafast response after photo-excitation in PTCDA thin films, which we address in this paper, has only recently been studied [13–15]. In the first part of this work, we present the progress of our detailed investigations [15] of the ultrafast excitonic intraband relaxation in $k-$space that follows from the negative exciton dispersion [16–20]. Photoinduced absorption in pump-probe spectroscopy was employed to show that the absorbing state is depopulated on a 100 fs time scale, and that this process depends on the initial excitation density.

The second part of this work deals with exciton-exciton annihilation in PTCDA at high excitation densities. We test diffusion models in both one and three dimensions as well as a single-step Förster-type mechanism. We extract values for annihilation rates, diffusion constants, diffusion lengths and Förster radii.

2. Annihilation models

First, we review the concepts of a bimolecular annihilation process applied in the second part of the paper. The general rate equation can be written as:

$$\frac{d}{dt}\,n(t) = -\frac{n(t)}{\tau} - f\,\gamma\,n(t)^2\ . \tag{1}$$

Here, $n(t)$ is the exciton density, τ a generalized exciton lifetime comprising radiative and nonradiative processes without bimolecular recombination (low density limit), and γ is the annihilation rate constant, which may be time-dependent. The factor f depends on the the type of annihilation reaction. First, we consider the reaction $\mathrm{S_1} + \mathrm{S_1} \rightarrow \mathrm{X} + \mathrm{S_0}$, where $\mathrm{S_0}$ is the ground state, $\mathrm{S_1}$ the first excited singlet state, and X a higher excited state. If no exciton remains after bimolecular annihilation, $f = 1$. This case applies if e.g. the excitons directly create an ionized state, which is typically assumed in the early works on molecular crystals [5]. If, however, the annihilation of a pair leaves one exciton behind $(\mathrm{S_1} + \mathrm{S_1} \rightarrow \mathrm{S_n} + \mathrm{S_0} \rightarrow \mathrm{S_1} + \mathrm{S_0})$, $f = 1/2$.

In the following, we discuss three different microscopic models for exciton-exciton annihilation: (i) three-dimensional diffusion, (ii) one-dimensional diffusion and (iii) single-step Förster transfer.

(i) Three-dimensional diffusion. In its simplest version, excitons are assumed to be particles with isotropic diffusion constant D, which annihilate if a pair comes closer than a critical distance $\bar{a}$. This distance corresponds to an average 3D-lattice constant. An approximate solution was already given for the equivalent problem of coagulating particles by Smoluchowski [21] and reviewed in, e.g., Ref. [22]:

$$\gamma_{\mathrm{3D}} = 8\pi D\bar{a}\left(1 + \frac{\bar{a}}{\sqrt{2\pi D t}}\right) \tag{2}$$

We briefly sketch the derivation of Eq. (2) in order to translate the ideas to the single-step mechanism (iii). The derivation is based on the related problem of particle capture by an immobile capturing center. Assuming an interaction distance $\bar{a}$ and an initially uniform exciton concentration n_0, the diffusion problem around the spherical quenching sphere of a single trap can be exactly solved and gives for the exciton current into the trap (e.g. [23]):

$$J = \gamma_{\mathrm{T3D}} \cdot n_0 \tag{3}$$

with a rate constant

$$\gamma_{\mathrm{T3D}} = 4\pi D\bar{a}\left(1 + \frac{\bar{a}}{\sqrt{\pi D t}}\right)\ . \tag{4}$$

Considering a number N_{T} of non-interacting traps within a volume V, the exciton number changes according to $\dot{N} = -N_{\mathrm{T}}J$, and the average exciton density $n = N/V$ is (with $n_{\mathrm{T}} = N_{\mathrm{T}}/V$):

$$\dot{n} = -\gamma_{\mathrm{T3D}} \cdot n_{\mathrm{T}} \cdot n_0\ . \tag{5}$$

This rate equation describes the diffusion of excitons driven by the concentration gradient between the inner boundary given by the trap-surface ($n(\bar{a}) = 0$) and the outer boundary given by the undisturbed region far away $n(r \rightarrow \infty) = n_0$. If additional processes change the concentration at the outer boundary, n_0 should be replaced by its actual value and can be approximated by the average concentration n:

$$\dot{n} = -\gamma_{\mathrm{T3D}} \cdot n_{\mathrm{T}} \cdot n\ . \tag{6}$$

The rate law (6) for the trapping problem can easily be used to describe the situation of exciton-exciton annihilation. Then, each exciton can act as a trap and $n_\mathrm{T} = n$. Note that this correspondence refers to an annihilation reaction of the type $\mathrm{S}_1 + \mathrm{S}_1 \rightarrow \mathrm{X} + \mathrm{S}_0$ (both excitons are destroyed) with $f = 1$. One might think at first glance that use of the trapping rate law implies a survival of one exciton (the trap). However, the annihilation of the trap is included by the fact that the concentration n of "excitons falling into the traps" refers to all excitons and thereby includes the "excitons acting as traps". In addition to setting $n_\mathrm{T} = n$, the rate constant γ_T3D for the diffusion current into the trap has to be modified, since now the trap itself is mobile. Since the relative motion of two diffusing particles can be described by an effective diffusion constant $D_\mathrm{eff} = D + D$ [21,22], the rate constant γ_T3D becomes γ_3D as given in Eq. (2).

In many cases, this rate constant (2) is considered only for time scales $t \gg \bar{a}^2/(2\pi D)$. Using the nearest neighbor hopping time $t_\mathrm{H} = \bar{a}^2/(6D)$, this corresponds to $t \gg t_\mathrm{H}$. At such time scales, the transient term in Eq. (2) can be neglected and the rate constant takes the simple, time-independent form $\gamma_\mathrm{3D} = 8\pi D\bar{a}$. Such a time-independent rate law provides the motivation for generally writing the annihilation rate law in the form of Eq. (1).

(ii) One-dimensional diffusion. The rate constants for diffusion-controlled reactions strongly depend on the dimensionality of the system [24]. In a molecular crystal, the diffusion constant might be strongly anisotropic and thus allow effective diffusion only along two or one dimensions. In the one-dimensional case, the rate constant for bimolecular annihilation is (given e.g. in [25]):

$$\gamma_\mathrm{1D} = \frac{1}{aN_0}\sqrt{\frac{8D}{\pi t}} \;, \tag{7}$$

with a being the 1D-lattice constant, D the exciton diffusion constant along the considered direction and N_0 the three-dimensional molecular density.

The rate constant (7) follows from the one-dimensional diffusion problem for a semi-infinite slab. For the initial condition $n(x, t = 0) = n_0$ and the boundary condition $n(x = 0, t) = 0$ (perfect sink at the surface of the slab), the exciton current density into the sink is $\sqrt{D/(\pi t)}$ [26]. One can now treat the 3D molecular crystal as a system of 1D stacks. Within these stacks, on assumes trapping sites (volume density n_T) which act as sinks in the 1D problem along the stack. In complete analogy to derivation of Eq. (6) one arrives at a rate law for the trapping problem in a quasi-one-dimensional material:

$$\dot{n} = -\gamma_\mathrm{T1D} \cdot n_\mathrm{T} \cdot n \;, \tag{8}$$

with

$$\gamma_\mathrm{T1D} = \frac{1}{aN_0}\sqrt{\frac{4D}{\pi t}} \tag{9}$$

As for the 3D case, the transition from the trapping problem (8) to the annihilation problem is done by taking $n_\mathrm{T} = n$ and by using the effective diffusion constant $D_\mathrm{eff} = D + D$ in the rate constant γ_T1D, arriving at the annihilation rate constant γ_1D in Eq. (7). In remarkable contrast to the 3D diffusion problem, the 1D rate constants γ_T1D and γ_1D (both for trapping and annihilation) do not approach a finite value for large t. Thus, the dynamics in 1D will be qualitatively different from the 3D case.

(iii) Single-step Förster transfer. The two diffusion models discussed so far assume that the excitons move like a random walker in many steps of the type $\mathrm{S}_1 + \mathrm{S}_0 \rightarrow \mathrm{S}_0 + \mathrm{S}_1$ towards each other, until they annihilate via a short range interaction in a final step of the type $\mathrm{S}_1 + \mathrm{S}_1 \rightarrow \mathrm{X} + \mathrm{S}_0$. As an alternative model, we now discuss the case that annihilation occurs without exciton diffusion and just by a single, long-range annihilation step.

PTCDA shows strong photoinduced absorption in the range of 1.7-2.0 eV (cf. Fig. 1b). This allows for good spectral overlap with the photoluminesence, which peaks at about 1.75 eV (not shown, see e.g. Ref. [14]). Thus, efficient Förster type energy transfer with large Förster radius R_F can be expected for the annihilation step $\mathrm{S}_1 + \mathrm{S}_1 \rightarrow \mathrm{S}_\mathrm{n} + \mathrm{S}_0$, with S_n being the final state in the pump-probe experiments.

To derive a rate law for such a single-step annihilation mechanism, we start again with the trapping problem. Förster [27] considered a model in which a donor molecule is surrounded by a statistic distribution of acceptor molecules (volume concentration n_T). For a single donor molecule, the decay rate follows from a summation of the intrinsic decay rate $1/\tau$ and all energy transfer rates to the surrounding acceptor molecules. Averaging over all distributions of donor molecules leads to the time dependent exciton population on the donor molecules [27]:

$$n(t) = n_0 \cdot \exp\left(-\frac{t}{\tau} - \frac{4}{3}\pi R_{\mathrm{F}}^3 \sqrt{\frac{\pi t}{\tau}} n_{\mathrm{T}}\right) . \tag{10}$$

Derivation with respect to t yields a rate equation

$$\dot{n} = -\frac{n}{\tau} - \gamma_{\mathrm{F}} \cdot n_{\mathrm{T}} \cdot n , \tag{11}$$

with a rate constant

$$\gamma_{\mathrm{F}} = \frac{2}{3}\pi\, R_{\mathrm{F}}^3 \sqrt{\frac{\pi}{\tau\, t}} . \tag{12}$$

The rate laws (11) or (10) are used to discuss luminescence quenching experiments in molecular crystals with an acceptor (quencher) concentration n_{T} [28]. For application to annihilation experiments, we identify $n_{\mathrm{T}} = n$ as in the diffusion problem and arrive at a rate law of the general form (1) with an annihilation constant given by (12). The obtained rate constant for the single-step annihilation mechanism is (apart from the role of τ) structurally equivalent to the rate constant for the 1D diffusion model. In particular, there is again no regime in which the rate constant would become time-independent as in the 3D diffusion model.

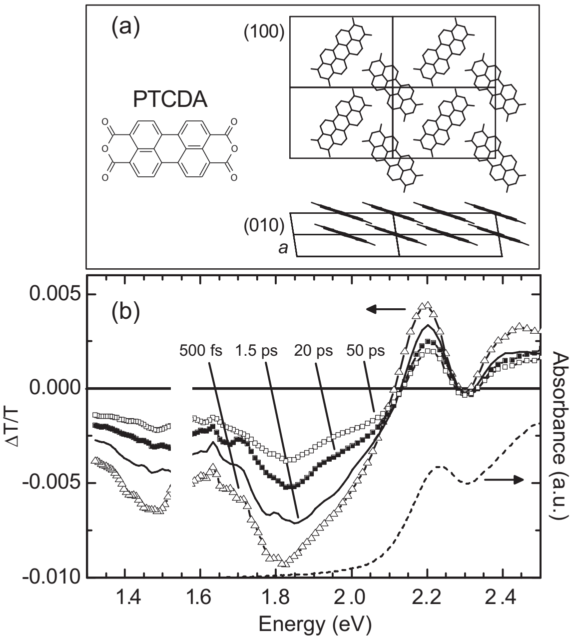

Fig. 1. (a) Molecular structure and crystal structure of α-PTCDA [29]. The direction of close stacking is [100] with a corresponding lattice constant of $a = 3.72\,\text{Å}$, much smaller than the other lattice constants ($b = 11.96\,\text{Å}$, $c = 17.34\,\text{Å}$). (b) Linear absorbance of a polycrystalline film at room temperature (dashed) and transient transmittance at different delays between pump and probe pulses. The spectrum around the fundamental amplifier output 1.55 eV is distorted and not shown.

3. Experimental

Our samples were polycrystalline films of PTCDA of ∼25 nm and ∼35 nm thickness which were grown by physical vapor deposition in high vacuum (10^{-6} mbar) on c-oriented sapphire substrates. Before deposition, the material was purified by gradient sublimation. AFM measurements revealed that the size of the crystallites was of the order of 100 nm. All measurements were carried out with an ultrafast pump-probe setup based on a 1 kHz Ti:sapphire regenerative amplifier, which was seeded by a home-built Ti:sapphire oscillator. A fraction of the 800 nm-output of 750 mW power pumped a home-built optical parametric amplifier in non-collinear geometry (N-OPA) [30]. Its linearly polarized output pulses were further compressed down to 22 fs by a prism compressor. The spectrum was shaped in the Fourier plane of the compressor and centered around 2.22 eV to excite at the lowest vibronic state of the S_0-S_1-transition (cf. dashed line in Fig. 1 (b)). In the following, this state is refered to as the absorbing state (at $k = 0$). Metallic neutral-density filters were employed to modify the pump power, from which excitation densities were estimated under assumption of a laser focus of 50 μm diameter on the (thin) sample. This diameter was measured as the FWHM of the Gaussian spot at the sample position.

The probe pulses originated from a femtosecond continuum, which was generated by focusing a small fraction of the amplifier output into a 2 mm sapphire plate. For the measurements of the annihilation properties and the initial ultrafast relaxation on short time scale, where high time resolution was required, an acousto-optical programmable dispersive filter [31] was used to shape both spectral phase and amplitude (Gaussian around 1.94 eV with about 100 meV FWHM). For the transient spectra, the full white-light spectrum between 500 nm and 950 nm was used, and the pump excitation density was $6 \times 10^{19}\,\mathrm{cm}^{-3}$. Spectral selection was performed after the sample with a monochromator. All data was recorded as differential transmission $\Delta T/T$, where ΔT is the pump-induced transmission change of the probe beam. For a better signal-to-noise ratio, an autobalanced photoreceiver (Si-PIN photodiodes) with a reference beam and lock-in detection at the laser frequency was employed. During the low-temperature measurements, the samples were kept in a Helium continuous-flow optical cryostat.

4. Results and discussion

Transient spectra. First, we discuss the initial ultrafast excitonic relaxation process after photoexcitation. This relaxation is interpreted as an intraband-relaxation in $k-$space from the Γ-point towards the border of the Brillouin zone [15].

As a prerequisite, fs-transient spectra were recorded to identify transitions $\mathrm{S_1}$-$\mathrm{S_n}$ into higher excited states giving rise to excited state absorption (ESA). Transient transmittance spectra are shown in Fig. 1 (b) for selected delays between pump and probe beam, recorded with a spectral resolution of $\sim 4\,\mathrm{nm}$. The spectra were corrected for the chirp present in the femtosecond continuum. Since the time resolution was about 200 fs, and because the discussion of the spectral shape is qualitative, we do not present spectra at delays smaller than 500 fs. By 500 fs, the spectra have already surpassed their maxima and relax thereafter. The spectra exhibit ground state bleaching ($\Delta T/T > 0$) in the region of linear absorption resembling its shape with peaks at 2.2 eV and 2.45 eV. One important exception is a dip at 2.30 eV, where $\Delta T/T < 0$, which we attribute to an underlying ESA transition with negative $\Delta T/T$. Furthermore, two broad ESA bands peaking at 1.48 eV and 1.82 eV can be clearly observed. No significant peak shifts with time that might indicate intraband relaxation are visible on this longer time scale.

Ultrafast intraband relaxation. In the following, the probe spectrum was centered around 1.94 eV to probe into the major ESA peak with a time resolution of 30 fs. Figure 2 shows $\Delta T/T$-data for three selected pump intensities, at 295 K and 5 K. For a better comparison, each curve has been normalized to its maximum value. For both temperatures, $S(t) = |\Delta T/T|$ starts to rise with time resolution, indicated by the dashed integrated cross-correlation curves. Yet, a subsequent delayed rise is clearly visible (except only for high intensity at 295 K) that slows down with both decreasing temperature and excitation intensity. After $|\Delta T/T|$ reached its maximum (which can be better seen on a longer time scale, cf. Fig. 3), it decays as a result of exciton recombination or annihilation, which is discussed in the next subsection.

When considering that two time constants are present in the data, the convolution

$$S(t) \propto \int_{-\infty}^{\infty} dt' XC(t-t')(1-\sum_{i=1,2} c_i\, e^{-t/\tau_i}) \qquad (13)$$

with the Gaussian cross-correlation envelope function $XC(t)$ allows us to fit curves to the data. The best fits (with $c_i = 0.5$) yield $\tau_1 \approx 30\,\mathrm{fs}$, and a varying τ_2. Because we observe two decay constants, we assume to probe two states simultaneously. The smaller τ_1 is of the order of time resolution, and the most straightforward conclusion is that it describes the initial excitation into the absorbing state. However, τ_2 certainly represents a time-resolved process, and we attribute it to the intraband relaxation in $k-$space, i.e., the depopulation of the $k = 0$ state towards the border of the Brillouin zone. In case of a multi-step relaxation, τ_2 is an upper limit for the depopulation of the absorbing state at $k = 0$.

Figure 2 (c) depicts the results for τ_2, which confirms that either temperature increase [32] or higher excitation accelerate the relaxation process. The relaxation in $k-$space requires the emission of phonons. Previous works, where the vibronic properties of PTCDA epitaxial films and single crystals have been investigated in detail, presented numerous vibronic modes that can possibly be emitted [33,34]. Phonon emission can be either spontaneous or stimulated by phonons already present in the crystal. The fact of faster relaxation at higher temperatures corresponds to increased stimulated phonon emission caused by a higher (thermal) concentration of stimulating phonons. Now, higher excitation density will also cause a higher phonon concentration and thus lead to increased stimulated phonon emission. Thus, all trends in Fig. 2 (c) can be qualitatively understood.

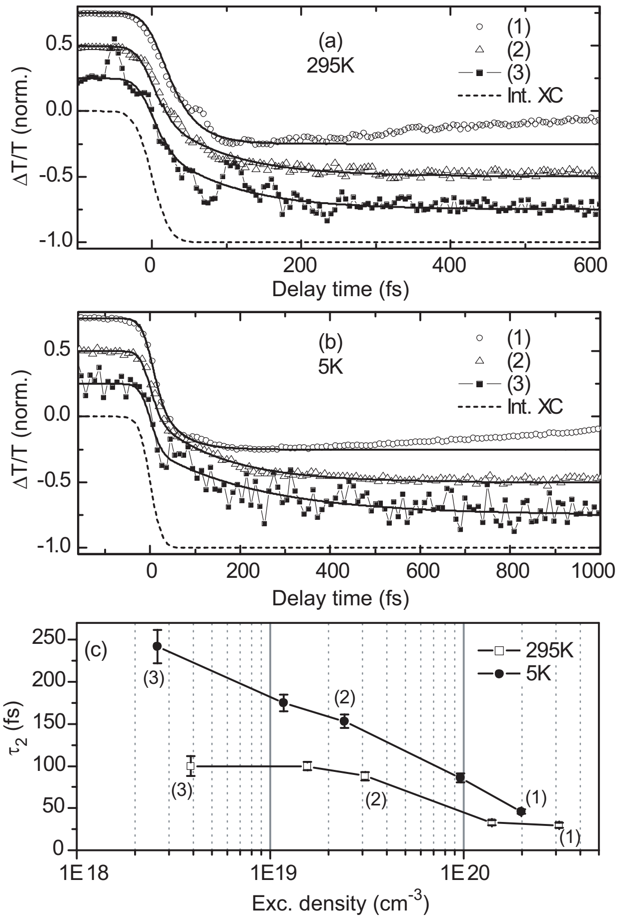

Fig. 2. Normalized differential transmittance for three selected pump intensities at 295 K (a) and 5 K (b). For clarity, the curves have been shifted vertically by 0.25 each. Solid lines are fit curves, the dashed lines are integrated cross-correlation curves. Excitation densities at 295 K (a) are: (1) 3.1×10^{20} cm^{-3}, (2) 3.1×10^{19} cm^{-3}, (3) 3.9×10^{18} cm^{-3}. At 5 K (b), the densities are (1) 2×10^{20} cm^{-3}, (2) 2.4×10^{19} cm^{-3}, (3) 2.6×10^{18} cm^{-3}. Graph (c) summarizes the relaxation time constant τ_2 as defined by Eq. (13).

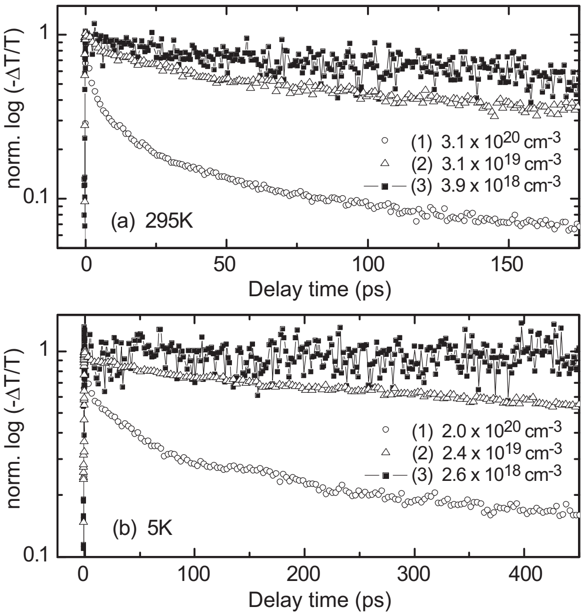

Fig. 3. Normalized differential transmission as a function of excitation density (as in Fig. 2) on a long time scale at 295 K (a) and 5 K (b).

However, it remains open whether the values of 100 fs at 295 K and 240 fs at 5 K for the lowest excitation densities of about $3 - 4 \times 10^{18}\,\mathrm{cm}^{-3}$ shown in Fig. 2 (c) are already the intrinsic low density limits. Ino and co-workers have reported upper and lower limits of 360 fs and 250 fs, respectively, for the relaxation time constant of the S_1 state at room temperature [13]. However, they did not mention excitation densities, and excitation took place into high energy-states of 5 eV. From the rise of photoluminescence [15], it can definitely be stated that the time constant for intraband relaxation is significantly faster than 5 ps (resolution limit).

Exciton-exciton interaction and annihilation. We now turn our attention towards the nature of de-excitation of excitons after the initial intraband relaxation. Figure 3 shows the data corresponding to Fig. 2 on a long time scale. Data for the negative $-\Delta T/T$ are presented on a logarithmic scale to elucidate that $\Delta T/T$ does not decay with a single exponential at moderate (2) and at high (1) excitation densities, whereas at the low density limit (3), $\log(-\Delta T/T)$ essentially shows linear behavior. We conclude that at densities higher than approximately 5×10^{18} cm^{-3}, exciton-exciton interaction must be considered, which leads to a deviation from a single-exponential decay. On a microscopic scale, the character of the interaction mechanism can be described by a diffusion-limited process or a static single-step reaction via Förster transfer, as introduced above.

In the following, we test all three models (i),(ii),(iii) to identify the most appropriate process by fitting curves to our data. To solve (1) with the corresponding annihilation constants γ_i (Eqns. (2),(7),(12)), we assumed the annihilation reaction $S_1 + S_1 \rightarrow S_n + S_0 \rightarrow S_1 + S_0$, i. e., $f = 1/2$ in Eq. (1). The results for the exciton density $n(t)$ are as follows:

$$n_{3\mathrm{D}}(t) = \frac{n_0\,\mathrm{e}^{-t/\tau}}{1 + c\left[\frac{\sqrt{2D\tau}}{\bar{a}}(1-\mathrm{e}^{-t/\tau}) + \mathrm{erf}\left(\sqrt{\frac{t}{\tau}}\right)\right]} \qquad (14)$$

for 3D diffusion (i), with $c = 4\pi n_0 \bar{a}^2 \sqrt{\frac{D\tau}{2}}$. Here, "erf" denotes the error function, which ist defined as

$$\mathrm{erf}(x) = \frac{2}{\sqrt{\pi}} \int\limits_0^x \exp^{-t^2} dt \quad . \qquad (15)$$

The low-density lifetimes τ were extracted from linear fits to the tail of the low-intensity curves $\log(\Delta T/T)$ (3) in Fig. 3 ($\tau_{5\mathrm{K}} \approx 5.7\,\mathrm{ns}$ and $\tau_{295\mathrm{K}} \approx 470\,\mathrm{ps}$). Fits were performed for distinct values of τ to estimate the error of the fit parameters.

For mapping excitation densities $n(t)$ to detected signals $\Delta T/T(t)$, we use a detection efficiency factor $\eta = |\Delta T/T|/n$. This factor can be determined from the known exciton density n_0 at $t = 0$ and is no fit parameter. The 3D-mean lattice constant $\bar{a}$ in PTCDA is $7.24\,\text{Å}$. Hence, only one parameter, the diffusion coefficient D, was fit at a time, making the fits more reliable.

For the other models, one obtains:

$$n_{1\mathrm{D}}(t) = \frac{n_0\,\mathrm{e}^{-t/\tau}}{1 + \frac{n_0}{aN_0}\sqrt{2D\tau}\;\mathrm{erf}\left(\sqrt{\frac{t}{\tau}}\right)} \qquad (16)$$

for 1D diffusion (ii), with 1D-lattice constant $a = 3.72\,\text{Å}$, and

$$n_{\mathrm{F}}(t) = \frac{n_0\,\mathrm{e}^{-t/\tau}}{1 + \frac{1}{3} n_0 R_{\mathrm{F}}^3 \pi^2\;\mathrm{erf}\left(\sqrt{\frac{t}{\tau}}\right)} \qquad (17)$$

for a single-step Förster process (iii). In the latter case, R_{F} was the (only) fit parameter.

Figure 4 shows the data for high (1) and moderate (2) excitation densities as in Fig. 3, together with the best fits for all three models. In all cases, the fit curves for the 1D-diffusion limited process are in very good agreement with the data. As expected from the same structure and $t^{-1/2}$-dependence of Eqns. (7),(12), this also applies to the Förster single-step model (curves coincide). In contrast, the 3D-diffusion model shows clear discrepancies. We interpret this result as an evidence that exciton transport in PTCDA — in case of a diffusion-limited process — is primarily one-dimensional, along the stacking direction. However, it cannot be excluded that exciton annihilation is due to a single-step Förster-type process.

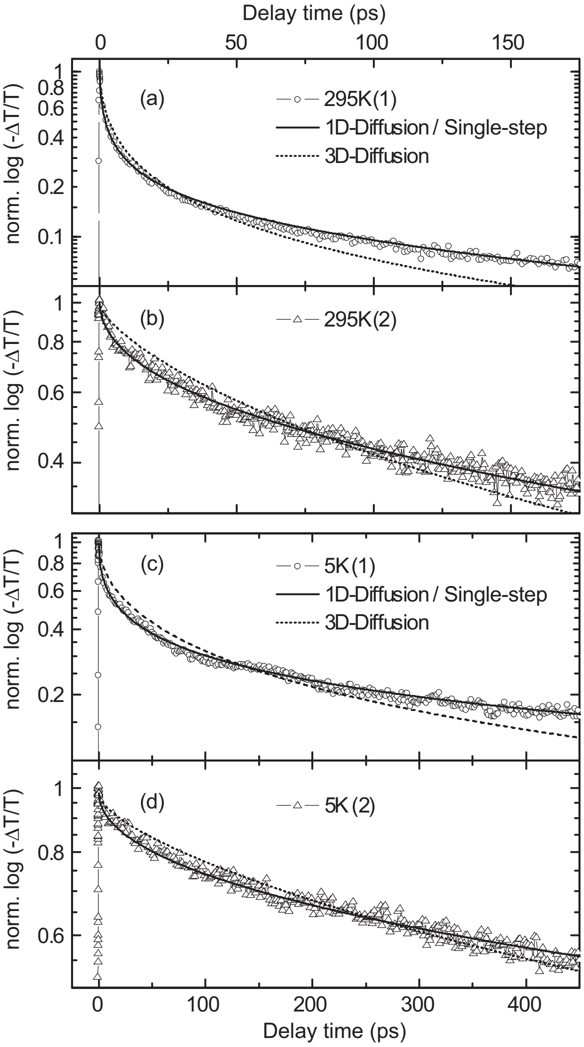

Fig. 4. Fits to selected data (1) and (2) of Fig. 3 for 295 K (a),(b) and 5 K (c),(d). Fit curves have been calculated as defined by (16) for 1D diffusion (straight line) and (14) for 3D-diffusion (dashed). Fit curves for single-step Förster after (17) coincide with curves for 1D diffusion. Excitation densities as in Figs. 2,3. Displayed results are from best fits. Note that the vertical scale differs between the four panels.

Results for the diffusion constants D and Förster radii R_{F} are shown in Fig. 5. For both room and low temperature, the obtained D are independent of the initial exciton density n_0. This proves that models (i) or (ii) can be consistently applied for various n_0. The temperature dependence of D shows an increase from $(5 \pm 1) \times 10^{-3}$ cm^{2}s^{-1} at Helium temperature to $(4 \pm 1) \times 10^{-2}$ cm^{2}s^{-1} at room temperature. These values correspond to annihilation rates $\gamma_{1\mathrm{D}} \approx 1.15 \times 10^{-15}\,\mathrm{t}^{-1/2}$ cm^{3}s$^{-1/2}$ and $\gamma_{1\mathrm{D}} \approx 3.2 \times 10^{-15}\,\mathrm{t}^{-1/2}$ cm^{3}s$^{-1/2}$ at 5 K and 295 K, respectively.

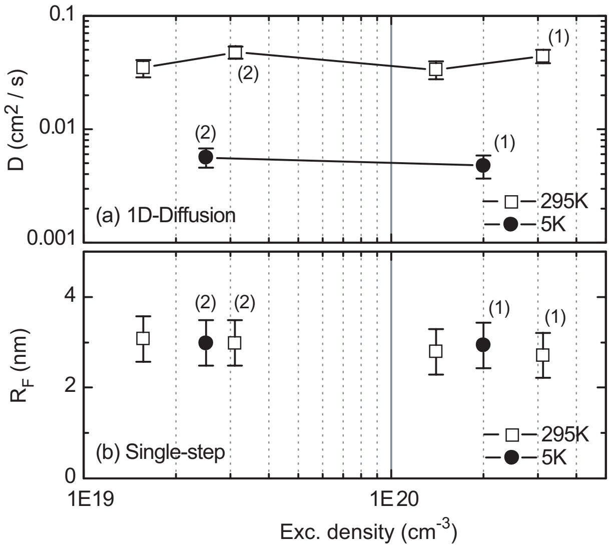

Fig. 5. Diffusion constants for the 1D-diffusion model (a) and Förster radii for the single-step Förster model (b). Open squares are at 295 K, solid circles are at 5 K. Excitation densities as in Figs. 2,3. Error bars indicate variations due to different values of the lifetime τ used in the fits.

Schüppel and co-workers [35] have extracted diffusion constants and diffusion lengths from luminescence quenching measurements in a PTCDA/TiOPC (titanyl-phthalocyanine) system and extracted values of 10^{-3} cm^{2}s^{-1} at 5 K and 6×10^{-3} cm^{2}s^{-1} at 295 K, which are smaller than our values by a factor of 5 to 7. The difference might be explained with the fact that the probed state in our experiments is likely to differ from the emitting state probed in the luminescence quenching measurements, so that a direct comparison of the values fails. Moreover, in our experiments, where we look at a shorter time window, we may see a higher effective D because fewer excitons have been bound by traps and impurities. Local heating effects alone, due to intense excitation, cannot be held responsible, as D does not depend on n_0.

A thermally activated hopping process may be regarded as the probable cause for the growth of D by one order of magnitude [23]. One should note that this increase in D goes in parallel with a decreased lifetime τ as a result of the activation of nonradiative decay channels. Therefore, the resulting root mean square displacement

$$\Lambda_{1\mathrm{D}} = \sqrt{2D\tau} \tag{18}$$

might eventually be independent of T, and we get $\Lambda_{1\mathrm{D}} \approx 75$ nm at 5 K and $\Lambda_{1\mathrm{D}} \approx 61$ nm at 295 K. Due to the uncertainty in the determination of several parameters, these values are approximate. Remarkably, the average distance of excitons in the stack at the highest excitation density ($n = 3.1 \times 10^{20}\,\mathrm{cm}^{-3}$) is about $\Delta x = aN_0/n = 3.1\,\mathrm{nm}$ and thereby much smaller than the root mean square displacement. Thus, one of the premises for the derivation of the annihilation constant is not fulfilled, namely the assumption of non-interacting traps. The nevertheless high accuracy of the fit might be explained by the arguments given in the derivation of the 3D-model for the case of overlapping diffusion regions. Alternatively, the underlying mechanism could be a single-step mechanism as discussed below. Interestingly, the diffusion constants exceed the ones obtained in a similar way for phthalocyanines, which are also quasi-1D materials, by one order of magnitude [6,7].

The Förster radii R_{F} for model (iii) are shown in Fig. 5 (b). The resulting R_{F} are all in the range of 3 ± 0.5 nm, which corresponds to annihilation rates of $\gamma_{\mathrm{F}} \approx 1.3 \times 10^{-15}\,\mathrm{t}^{-1/2}$ cm^{3}s$^{-1/2}$ (5 K) and $\gamma_{\mathrm{F}} \approx 4.7 \times 10^{-15}\,\mathrm{t}^{-1/2}$ cm^{3}s$^{-1/2}$ (295 K). As for D in the diffusion model, the R_{F} obtained do not depend on the initial exciton density n_0 for both room and Helium temperature, which confirms the consistency of the model. In addition, it can be seen that the R_{F} are also independent of T. Temperature-independent values for R_{F} are consistent with temperature-independent values for the diffusion length Λ in the 1D-model, since both parameters describe an effective length-scale for the interaction.

A temperature-independent R_{F} is physically reasonable for the assumed Förster transfer: Because the $\mathrm{S}_1 \rightarrow \mathrm{S}_0$ emission spectrum overlaps well with the $\mathrm{S}_1 \rightarrow \mathrm{S}_\mathrm{n}$ absorption, a temperature dependent change of the shape of the spectra will have no strong impact on the spectral overlap integral, which determines the Förster transfer rate. The good spectral overlap, together with the fact that both transitions are strongly allowed singlet-singlet transitions, can also explain the large value of R_{F}. It is similar to Förster radii in effective donor-acceptor energy transfer systems, since essentially the same type of transitions is involved. This is in contrast to the mechanism of a nearest-neighbor jump in the diffusion model: For this jump, the spectral overlap between $\mathrm{S}_1 \to \mathrm{S}_0$ emission and $\mathrm{S}_0 \to \mathrm{S}_1$ absorption has to be considered (jump to an un-excited molecule). Because of the large Stokes-shift, this overlap is formed by the wings of two well separated peaks and it is strongly influenced by temperature dependent changes in the peak-width. Rising temperature gives broader spectra, larger overlap and finally larger diffusion constants.

For completeness, we also list the diffusion constants D obtained within the 3D-model: $D = (6.4 \pm 0.4) \times 10^{-5}$ $\mathrm{cm}^2\mathrm{s}^{-1}$ at 5 K and $D = (3 \pm 0.3) \times 10^{-4}$ $\mathrm{cm}^2\mathrm{s}^{-1}$ at 295 K, which corresponds to annihilation constants $\gamma_{3\mathrm{D}} \approx 1.2 \times 10^{-10}$ $\mathrm{cm}^3\mathrm{s}^{-1}$ and $\gamma_{3\mathrm{D}} \approx 5.5 \times 10^{-10}$ $\mathrm{cm}^3\mathrm{s}^{-1}$, respectively. It is also worth mentioning that for excitation densities higher than about $10^{21}\,\mathrm{cm}^{-3}$ (data not shown), the 3D model performs better than for lower densities. We assume that this is due to an increased interaction between adjacent stacks, so that interstack hopping may occur. The hopping times at 295 K are $t_{\mathrm{H}} = \bar{a}^2/(6D) = 2.9\,\mathrm{ps}$ and thus relatively short compared to the timescale that we investigate. Thus, in our regime the transient term in the 3D annihilation rate constant (2) is indeed only a minor correction ($\mathcal{O}(10^{-6})$).

Larger corrections would be expected from other approximations inherent in the simple 3D model (2): The obtained diffusion constants correspond to root mean square displacements (in the 3D case) of

$$\Lambda_{3\mathrm{D}} = \sqrt{6D\tau}\ , \tag{19}$$

which gives values of 9 nm at 295 K or 15 nm at 5 K. These root mean square displacements are only one order of magnitude above the average lattice constant $\bar{a} = 7.24$ Å and thus the continuum approximation in the 3D diffusion model becomes already crude. Furthermore, $\Lambda_{3\mathrm{D}}$ is only a factor of two above the Förster radius obtained from the single step model. Alternatively expressed, the number of single diffusion steps during the exciton life time is only e.g. 160 at 295 K. For such a small number of diffusion steps, a distinction between pure diffusion models and long-range single step models becomes difficult and combined models would be most appropriate as e.g. discussed for the trapping problem in [5]. These problems of the 3D-diffusion results do much less arise in the 1D-diffusion model, since there the obtained displacements are much larger and the number of single diffusion steps is of the order of ~ 27000 at 295 K, providing internal consistency to the 1D-diffusion model.

5. Conclusion

In conclusion, we have shown how the relaxation processes in the perylene derivative PTCDA are affected by excitation density and temperature. We present transient spectra of PTCDA thin films. The spectra exhibit ground state bleaching contributions, corresponding to the shape of linear absorption, and three broad excited state transitions. The dynamics of the major excited state transition was used to analyze the ultrafast intraband relaxation from the absorbing state at $k = 0$ to the border of the Brillouin zone. The relaxation becomes faster with rising temperature or with higher excitation density probably due to stimulated emission of phonons.

At excitation densities above about $10^{19}\,\mathrm{cm}^{-3}$, exciton-exciton annihilation is the major decay mechanism of the relaxed excitons. The experimental decay dynamics can be explained with high precision by two alternative annihilation models: one-dimensional diffusion limited bimolecular recombination or single-step long range Förster-type annihilation. Both models predict the same type of decay law with essentially one free parameter: diffusion constant D or Förster radius R_{F}. With this one parameter, a whole set of intensity-dependent multi-exponential decay curves can be consistently fitted. Temperature dependence and order of magnitude of the obtained parameters D or R_{F} correspond to expectations in both models. Thus, a decision between them cannot be made based on our data. The three-dimensional annihilation law (2), which was extensively used in polyacene crystals [5], is significantly less adequate to describe the decay data.

6. Acknowldgement

We thank Deutsche Forschungsgemeinschaft (projects HA 3280/1, HO 2450/1, Leibniz award) for financial support.

References

[1] C. W. Tang, Appl. Phys. Lett. **48** (1986) 183.

[2] C. W. Tang and S. A. VanSlyke, Appl. Phys. Lett. **51** (1987) 913 ; J. H. Burroughes *et al.*, Nature **347** (1990) 539 .

[3] M. A. Baldo and S. R. Forrest, Phys. Rev. B **62** (2000) 10958; M. A. Baldo, C. Adachi and S. R. Forrest, Phys. Rev. B **62** (2000) 10967.

[4] M. A. Baldo, R. J. Holmes and S. R. Forrest, Phys. Rev. B **66** (2002) 035321.

[5] R. C. Powell and Z. G. Soos, J. Lumin. **11** (1975) 1.

[6] B. I. Greene and R. R. Millard, Phys. Rev. Lett. **55** (1985) 1331.

[7] V. Gulbinas, M. Chachisvilis, A. Persson, S. Svanberg, and V. Sundström, J. Phys. Chem. **98** (1994) 8118; V. Gulbinas, M. Chachisvilis, L. Valkunas, and V. Sundström, J. Phys. Chem. **100** (1996) 2213.

[8] V. Sundström, T. Gillbro, R. A. Gadonas, and A. Piskarskas, J. Chem. Phys. **89** (1988) 2754.

[9] I. V. Ryzhov, G. G. Kozlov, V. A. Malyshev, and J. Knoester, J. Chem. Phys. **114** (2001) 5322.

[10] E. S. Maniloff, V. I. Klimov, and D. W. McBranch, Phys. Rev. B **56** (1997) 1876.

[11] E. Hädicke and F. Graser, Acta Cryst. C **42** (1986) 189.

[12] S. R. Forrest, Chem. Rev. **97** (1997) 1793.

[13] D. Ino, K. Watanabe, N. Takagi,and Y. Matsumoto, Chem. Phys. Lett. **383** (2004) 261.

[14] E. Engel, M. Koschorreck, K. Leo, and M. Hoffmann, J. Lumin. **112** (2005) 299.

[15] E. Engel, M. Koschorreck, K. Leo, and M. Hoffmann, Phys. Rev. Lett., in press.

[16] M. H. Hennessy, Z. G. Soos, R. A. Pascal Jr., and A. Girlando, Chem. Phys. **245** (1999) 199.

[17] M. Hoffmann and Z. G. Soos, Phys. Rev. B **66** (2002) 024305.

[18] M. Hoffmann, Z. G. Soos, and K. Leo, Nonl. Opt. **29** (2002) 227.

[19] I. Vragović and R. Scholz, Phys. Rev. B **68** (2003) 155202.

[20] G. Mazur, P. Petelenz, and M. Slawik, J. Chem. Phys. **118** (2003) 1423.

[21] M. v. Smoluchowski, Z. Physik. Chemie (Leipzig) **92** (1917) 129.

[22] S. Chandrasekhar, Rev. Mod. Phys. **15** (1943), 1.

[23] V. M. Agranovich and M. D. Galanin, Electronic Excitation Energy Transfer in Condensed Matter, North-Holland Amsterdam, 1982.

[24] A. Suna, Phys. Rev. B **1** (1970) 1716.

[25] D. C. Torney and H. M. McConnell, J. Phys. Chem. **87** (1983) 1941.

[26] H. S. Carslaw and J. C. Jaeger, Conduction of Heat in Solids, Clarendon Press, Oxford, 1959.

[27] T. Förster, Z. Naturforsch. **4a** (1949) 321.

[28] R. C. Powell, Phys. Rev. B **2** (1970), 2090.

[29] A. J. Lovinger, S. R. Forrest, M. L. Kaplan, P. H. Schmidt, and T. Venkatesan, J. Appl. Phys. **55** (1984) 467.

[30] T. Wilhelm, J. Piel, and E. Riedle, Opt. Lett. **22** (1997) 1494.

[31] P. Tournois, Opt. Comm. **140** (1997) 245.

[32] In a previous work, where the excitation intensity has not been as thoroughly controlled as in the current work, no temperature dependence has been observed [14].

[33] R. Scholz, A. Yu. Kobitski, T. U. Kampen, M. Schreiber, D. R. T. Zahn, G. Jungnickel, M. Elstner, M. Sternberg, and Th. Frauenheim, Phys. Rev. B **61** (2000) 13659.

[34] D. A. Tenne, S. Park, T.U. Kampen, A. Das, R. Scholz, and D.R.T. Zahn, Phys. Rev. B**61** (2000) 14564.

[35] R. Schüppel, T. Dienel, K. Leo, and M. Hoffmann, J. Lumin. **110** (2004) 309.

Notes to preprint-version added after publication

Update of Ref. [15]:

[15] E. Engel, M. Koschorreck, K. Leo, and M. Hoffmann, Phys. Rev. Lett. **95** (2005), 157403.